

High Quality QCD Axion at Gravitational Wave Observatories

Ricardo Z. Ferreira,^{1,*} Alessio Notari,^{2,†} Oriol Pujolàs,^{1,‡} and Fabrizio Rompineve^{3,§}

¹*Institut de Física d'Altes Energies (IFAE) and The Barcelona Institute of Science and Technology (BIST),
Campus UAB, 08193 Bellaterra, Barcelona, Spain*

²*Departament de Física Quàntica i Astrofísica & Institut de Ciències del Cosmos (ICCUB),
Universitat de Barcelona, Martí i Franquès 1, 08028 Barcelona, Spain*

³*Institute of Cosmology, Department of Physics and Astronomy, Tufts University, Medford, MA 02155, USA*

(Dated: April 15, 2022)

The axion solution to the strong CP problem is delicately sensitive to Peccei-Quinn breaking contributions that are misaligned with respect to QCD instantons. Heavy QCD axion models are appealing because they avoid this so-called “quality problem”. We show that generic realizations of this framework can be probed by the LIGO-Virgo-KAGRA interferometers, through the stochastic gravitational wave (GW) signal sourced by the long-lived axionic string-domain wall network, and by upcoming measurements of the neutron and proton Electric Dipole Moments. Additionally, we provide predictions for searches at future GW observatories, which will further explore the parameter space of heavy QCD axion models.

Introduction—A great amount of experimental effort has been aiming at discovering the QCD axion [1, 2], the pseudo-Goldstone boson of a spontaneously broken axial $U(1)$ Peccei-Quinn (PQ) symmetry [3, 4] that explains the smallness of CP violation in strong interactions.

While attractive, the PQ mechanism is vulnerable to possible additional sources of symmetry breaking, generically misaligned with respect to the axion potential from QCD instantons. This *quality problem* (originally formulated with various perspectives in [5–11]) is alleviated in *heavy axion* models (see [6] and [12–14] for earlier related work), where a “heavy QCD” sector provides a larger contribution to the axion potential, aligned with that from QCD instantons.

Existing realizations of this idea rely on: the QCD coupling becoming strong at high energies [6, 15–19], see also [20] for a 5D model; a separate confining gauge group, whose alignment is ensured by unification at high scales [14, 21–23] or by a softly-broken \mathbb{Z}_2 symmetry [24–26]. When the strong coupling scale Λ_H of the heavy sector is above the QCD scale Λ_{QCD} , the axion mass is larger than in the standard window, and the cosmological evolution of the axion field in the early Universe is shifted to higher energy scales. Despite its appeal, it is not immediately clear what the signatures of such a scenario are since generically the axion can be very heavy, e.g. above the electroweak scale, while its interactions remain very weak.¹ Furthermore, in contrast to the standard case, a heavy QCD axion can easily decay in the early Universe, and thus leaves no detectable relic dark matter today.

Nonetheless, in this Letter we show that heavy

QCD axion models can be observationally probed at gravitational wave (GW) observatories (already at the currently operating LIGO-Virgo-KAGRA (LVK) [29–31] interferometers), with the exciting possibility of a correlated signature in upcoming neutron and proton Electric Dipole Moment (nEDM, pEDM) measurements [32, 33].

GWs are indeed radiated [34] by the network of axionic topological defects (domain walls attached to strings) [35] (see also [36]), which are abundant in the early Universe if the PQ symmetry is broken after inflation. In standard QCD axion models the network necessarily annihilates while making up only a very tiny fraction of the energy density of the Universe, and therefore the GW signal is too weak to be detectable [37]. In contrast, the heavy QCD axion network can carry much more energy because of its larger domain wall tension. Furthermore, in generic realizations (e.g. DFSZ [38, 39] and simple generalizations of KSVZ models [40, 41]), the network can be long-lived while still avoiding the overproduction of relics, since radiated axion quanta are unstable. Annihilation of the network can be triggered by the misaligned PQ breaking effects that motivate the scenario in the first place (see [42]). These also induce a small but potentially observable shift of the QCD vacuum angle.

Our work points out a new source of observable gravitational waves from the dynamics of the QCD axion (see e.g. [43–46] for previous work, unrelated to the axion quality problem and [47–50] for related scenarios with ALPs).

The Heavy QCD Axion—Heavy QCD axion models are characterized by an extra contribution to the axion potential that is larger than and aligned with the contribution from QCD. The zero temperature potential is

$$V_a = \left(\kappa_{\text{QCD}}^2 \Lambda_{\text{QCD}}^4 + \kappa_H^2 \Lambda_H^4 \right) \left(1 - \cos \frac{a}{f} \right), \quad (1)$$

where f is the axion decay constant, $\Lambda_{\text{QCD,H}}$ denote

* rzambujal@ifae.es

† notari@fqa.ub.edu

‡ pujolas@ifae.es

§ fabrizio.rompineve@tufts.edu

¹ Axion masses and decay constants around or below the TeV scale can be probed at colliders, see e.g. [26–28].

the strong coupling scale of QCD and the heavy sector respectively, and $\kappa_{\text{QCD,H}} \leq 1$ are prefactors that depend on details such as the fermionic spectrum. For instance, QCD gives $\kappa_{\text{QCD}} \simeq (m_u/\Lambda_{\text{QCD}})^{1/2}$ with m_u the up quark mass. In explicit realizations of such scenarios [6, 14–18, 20–26] $\kappa_{\text{H}} \ll 1$ can similarly arise by the presence of a light quark in the heavy sector. Having QCD subdominant, the axion mass is dictated by the heavy sector as

$$m_a \simeq 10^8 \text{ GeV} \left(\frac{10^{12} \text{ GeV}}{f} \right) \left(\frac{\Lambda_{\text{H}}}{10^{10} \text{ GeV}} \right)^2 \kappa_{\text{H}}. \quad (2)$$

For our discussion, it is important to recall that gauge instantons generically break the original $U(1)$ PQ symmetry to a discrete $\mathbb{Z}_{N_{\text{DW}}}$ subgroup, where N_{DW} is a model-dependent integer number related to the axion coupling to gluons. Therefore the periodicity $2\pi f$ induced by the potential (1) can be smaller than the fundamental axion field range $2\pi f N_{\text{DW}}$ and the potential V_a can feature N_{DW} degenerate minima. In writing (1), we assumed that the periodicity induced by the heavy sector coincides with that of QCD instantons. This appears to be linked to the requirement of alignment between the two sectors, as is evidently the case in constructions with a \mathbb{Z}_2 symmetry [26] and in simple unification frameworks where SM and heavy sector fermions descend from the same fundamental representation of a higher-rank gauge group [18, 22]. This feature implies that the low-energy QCD-induced potential does not lift the degeneracy of the N_{DW} minima.

Generically, however, we may expect further contributions to the axion potential, misaligned with V_a . Independently of its specific origin, such a contribution can be written as

$$V_b \simeq -\mu_b^4 \cos \left(\frac{N_b}{N_{\text{DW}}} \frac{a}{f} - \delta \right), \quad (3)$$

where N_b defines the subgroup \mathbb{Z}_{N_b} of the PQ symmetry which is preserved by (3) and δ is a CP violating phase. In the absence of tuning, this offset is naturally $O(1)$ and $\mu_b \ll \Lambda_{\text{H}}$ is required to solve the strong CP problem. The low temperature potential is $V = V_a + V_b$ and when $N_b = 1$ or is co-prime with N_{DW} , the degeneracy of the N_{DW} minima is lifted. In particular, the vacuum energy difference between the global CP preserving minimum and its nearest neighbor is of the order $\Delta V \simeq \mu_b^4 [1 - \cos(2\pi N_b/N_{\text{DW}})]$ (provided that δ is not too close to π/N_{DW}). Broadly speaking, (3) can originate at a scale Λ_b , such that $\mu_b = \kappa_b^{1/2} \Lambda_b$. $\Lambda_b \gg f \gg \Lambda_{\text{H}}$ can arise from UV physics via: non-perturbative effects, $\kappa_b \sim e^{-S/2}$ (see e.g. [51–53]); higher-dimensional operators when the axion is the phase of a complex scalar field (see e.g. [9]); another gauge sector with confinement scale Λ_b and a light fermion of mass m_q , $\kappa_b \sim (m_q/\Lambda_b)^{1/2}$. $\Lambda_b \ll \Lambda_{\text{H}}$ can also arise from a confining gauge sector. Further details are provided in Appendix A.

Despite its smallness, a contribution from (3) can lead to potentially observable CP violation. In particular, at low temperatures one finds:

$$\Delta\theta \equiv \theta - \theta_{\text{QCD}} \simeq r^4 \left(\frac{N_b}{N_{\text{DW}}} \right) \left(\frac{\sin \delta}{\kappa_{\text{H}}^2} \right), \quad (4)$$

where $r \equiv \mu_b/\Lambda_{\text{H}}$. Current bounds from nEDM measurements [54] require $\Delta\theta \lesssim 10^{-10}$. Clearly, (4) shows that $\Lambda_{\text{H}} \gg \Lambda_{\text{QCD}}$ makes the PQ mechanism more robust against misaligned contributions.

In the early Universe, the mass m_a and the scale μ_b are generally temperature-dependent, for instance in the standard QCD axion case $m_a(T) \simeq m_a(T_0/T)^4$ for $T \geq T_0 \simeq 134 \text{ MeV}$ and $m_a(T) = m_a$ otherwise [55]. Nonetheless, our results are mostly independent of the detailed temperature dependence.

Axionic Defects—Let us now move to the cosmological evolution of topological defects, whose history begins at the PQ symmetry breaking scale $\sim N_{\text{DW}}f$. Our investigation concerns scenarios where this occurs during radiation domination after inflation, which will be generic for the values of f considered in this work.

Axionic strings form at $T \lesssim N_{\text{DW}}f$ and continuously radiate axion quanta and gravitational waves. In the absence of significant friction due to the plasma, they quickly achieve a scaling regime [56, 57] (see also [58] and [59–62] for recent updates), with energy density scaling as $\rho_s = \lambda \mu H^2$, with λ a $O(1)$ parameter and $\mu \sim N_{\text{DW}}^2 f^2$ the string tension.

This behavior is altered once $3H \simeq m_a(T)$. This occurs at a temperature $T_{\text{osc}} \gtrsim \Lambda_{\text{H}}$ (see Appendix B) when the axion field, with average initial value $a_i/(N_{\text{DW}}f) \sim O(1)$, starts oscillating in its potential V_a and domain walls form, attached to the strings, with a tension $\sigma \simeq 8m_a(T)f^2$. At this epoch, two possibilities arise: i) when $N_{\text{DW}} = 1$, the network of topological defects is rapidly annihilated by string-wall interactions (see e.g. [58]); ii) when $N_{\text{DW}} > 1$, the network persists because multiple domain walls pull each string in different directions.

In both cases, the tension of the walls is larger than in the standard QCD axion case by a factor $\Lambda_{\text{H}}/\Lambda_{\text{QCD}} \gg 1$. For $N_{\text{DW}} > 1$, in the absence of significant friction from the plasma (we show in Appendix D that this has a minor impact on our conclusions), the network rapidly achieves a scaling regime, with its energy density dominated by domain walls, $\rho_{\text{dw}} \simeq c\sigma H$, where c is a $O(1)$ numerical prefactor (in this regime V_a is normally already temperature-independent). This scales slower than matter and radiation and thus the network is potentially dangerous for cosmology [63]. However, domain wall domination can be generically avoided in the heavy axion scenario, thanks to the misaligned potential contribution V_b . The resulting vacuum pressure causes the contraction of the false vacuum regions and the collapse of the network [36] at a temperature T_{ann} , which can be estimated by imposing $\rho_{\text{dw}} \simeq \Delta V$ and more precisely determined via numerical simulations [64]. Here we

focus on the case where V_b is temperature-independent below Λ_H , as occurs generically when PQ breaking is due to physics above Λ_H , see Appendix B for the temperature-dependent case. To set ideas and simplify expressions, in the following we set $N_b = 1, N_{\text{DW}} = 6$ as example values, fix numerical prefactors according to the simulations of [64] and also fix the number of (entropy) relativistic degrees of freedom at T_{ann} to the SM value at high temperatures ($g_{*s, \text{ann}} g_{*, \text{ann}} = 106.75$ (see also Appendix B), although our results are only mildly affected by these precise choices. We then find

$$T_{\text{ann}} \simeq \frac{10^7 \text{ GeV}}{\sqrt{\kappa_H}} \sqrt{\frac{10^{12} \text{ GeV}}{f}} \left(\frac{\Lambda_H}{10^{10} \text{ GeV}} \right) \left(\frac{r}{0.005} \right)^2 \quad (5)$$

showing that for $r \ll 1$ network annihilation is significant delayed.

At (5) the network collapses and its energy density is transferred mostly to mildly relativistic axion quanta (see e.g. [58] and [64]). In contrast to the standard QCD axion case, in the heavy axion scenario these relics can efficiently decay to SM gluons, above the QCD Phase Transition (PT) and to photons and/or fermions, above and below the QCD PT, depending on the specific axion model. Focusing on the decay to gluons, since $m_a \gg \text{GeV}$ in most of the parameter space of interest [65], we find that decay is efficient below the temperature

$$T_{a \rightarrow gg} \simeq 10^7 \text{ GeV} \alpha_s \left(\frac{\sqrt{\kappa_H} \Lambda_H}{10^{10} \text{ GeV}} \right)^3 \left(\frac{10^{12} \text{ GeV}}{f} \right)^{\frac{5}{2}} \quad (6)$$

obtained by setting $\Gamma_{a \rightarrow gg} \simeq H$ (see Appendix B). This temperature can be larger than T_{ann} for $r \lesssim 0.001$ and/or $f \lesssim 10^{12} \text{ GeV}$. Therefore, axion relics from the network will in general decay immediately.

Crucially, however, the string-wall network can source a significant relic abundance of gravitational waves [70–76]. The simple quadrupole estimate for their energy density $\rho_{\text{gw}}(T_{\text{ann}}) \sim c^2 \sigma^2 / (32\pi M_p^2)$ has been confirmed by numerical simulations [76] (see also [37]). Assuming a standard radiation-dominated cosmological history after domain wall annihilation, one finds that the relic abundance of gravitational waves today is

$$\Omega_{\text{gw}} h^2 \simeq 0.01 (\Omega_{\text{rad}}^0 h^2) \tilde{\epsilon} \left(\frac{\rho_{\text{dw}}}{\rho_{\text{rad}}} \right)_{T=T_{\text{ann}}}^2, \quad (7)$$

where $\tilde{\epsilon} \simeq 0.1 - 1$ is a numerical efficiency factor [76] and ρ_{rad} and $\Omega_{\text{rad}} h^2 \simeq 4 \cdot 10^{-5}$ are the energy density and relic abundance of radiation today respectively. The formula above shows that when the network makes up $\gtrsim O(5\%)$ fraction of the energy density of the Universe at annihilation, its gravitational wave signal is detectable by present interferometers, i.e. $\Omega_{\text{gw}} h^2 \sim 10^{-9}$. This fraction at the annihilation temperature reads

$$\frac{\rho_{\text{dw}}}{\rho_{\text{rad}}} \Big|_{T=T_{\text{ann}}} \simeq 0.1 \kappa_H^2 \left(\frac{f}{10^{11} \text{ GeV}} \right)^2 \left(\frac{0.003}{r} \right)^4, \quad (8)$$

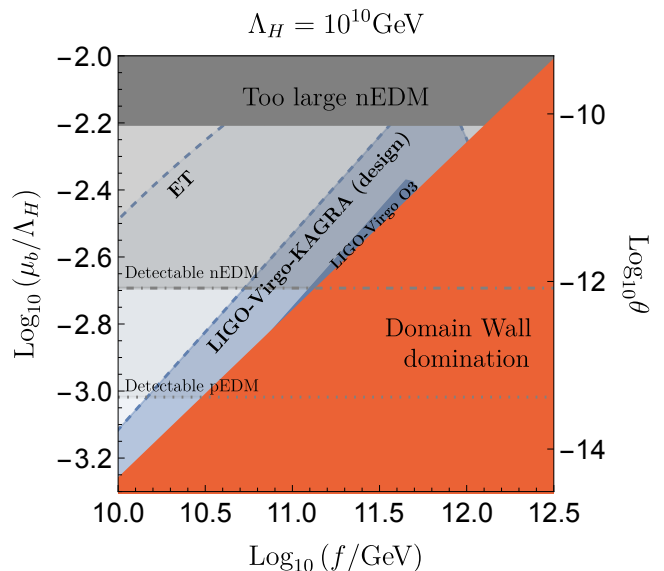


Figure 1. Regions of parameter space that can be probed by GW and/or nEDM experiments, for $\Lambda_H = 10^{10} \text{ GeV}$ and $\kappa_H = 1$. Constraints are also shown, as dark-shaded regions, from: domain wall domination (lower right corner), nEDM [54] (upper part), LIGO-Virgo O3 run [66] (dark-blue shaded). Dashed contours bound regions probed by LVK at design sensitivity and ET (sensitivity curves taken from [67]). The gray shaded region will be also probed by neutron [68] (dot-dashed line) and proton EDM [69] measurements.

for our example choice $N_b = 1, N_{\text{DW}} = 6$.

The GW signal is peaked at a frequency corresponding to H at annihilation (see e.g. [37]). Redshifted to today:

$$\omega_{\text{peak}} \simeq \frac{5 \text{ Hz}}{\sqrt{\kappa_H}} \left(\frac{r}{0.005} \right)^2 \left(\frac{\Lambda_H}{10^{10} \text{ GeV}} \right) \sqrt{\frac{10^{11} \text{ GeV}}{f}}. \quad (9)$$

According to (7), (8) and (9), the signal from a heavy axion with $f \lesssim 10^{11} \text{ GeV}$, $\Lambda_H \gtrsim 10^{10} \text{ GeV}$ and $r \gtrsim 10^{-3}$ sits right in the reach of the LVK interferometers [77, 78].

The GW spectrum away from the peak frequency [37] decreases as ω^3 for $\omega < \omega_{\text{peak}}$, whereas for $\omega > \omega_{\text{peak}}$ it behaves as $\sim \omega^{-1}$, until a cutoff frequency corresponding to the domain wall width. However, further numerical simulations are required to understand the precise behavior of the spectrum around the peak frequency.

Predictions—Although the $N_{\text{DW}} = 1$ case does not leave observable GW signals (see Appendix E) due to the quick decay of the network, the situation is radically different for $N_{\text{DW}} > 1$, where network annihilation is delayed. To simplify the presentation, we fix $N_b = 1, N_{\text{DW}} = 6, \kappa_H = 1$ and $g_{*, \text{ann}} = g_{*s, \text{ann}} = 106.75$ (see Appendix B for the case $\kappa_H \ll 1$) and $\delta = 0.3$ and present results varying $\Lambda_H, r \equiv \mu_b/\Lambda_H$ and f . According to (4), r can then be traded for $\Delta\theta$.

We first present results for large values of Λ_H , which maximally reduce the sensitivity to misaligned contributions.

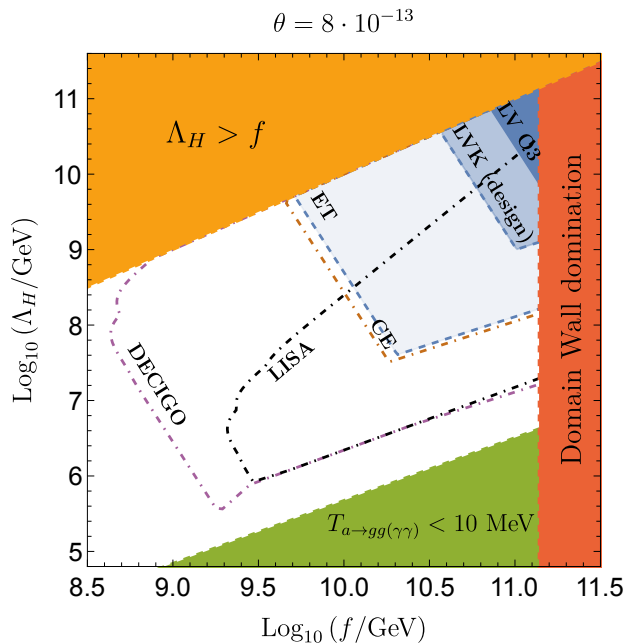


Figure 2. Regions of parameter space detectable at GW observatories, fixing $\theta = 8 \times 10^{-13}$ according to upcoming nEDM measurements [68] and $\kappa_H = 1$. Same description and color code as in Fig. 1, with the addition of CE, LISA and DECIGO’s sensitivity curves (dot-dashed, taken from [67]) and two constraints (dark-shaded regions) corresponding to axions decays below 10 MeV (lower right corner) and to $\Lambda_H > f$ (upper left corner).

We consider V_b to be temperature-independent at $T \lesssim \Lambda_H$ and Λ_H to have a QCD-like temperature behavior (see also Appendix C).

Fixing $\Lambda_H = 10^{10}$ GeV as a representative example, we show values of r and f that can be probed by gravitational wave observatories (dashed contours), together with constraints (solid contours), in Fig. 1. In the lower right half, the string-wall network dominates before annihilation. While this region might not be completely ruled out, annihilation of the network in this case would require a dedicated study. In the upper part of the parameter space the PQ solution is spoiled, i.e. $\Delta\theta \gtrsim 10^{-10}$ [54]. In the dark blue shaded region the GW signal is incompatible with the latest 2σ upper bound from LIGO-Virgo (LV) [66], this corresponds to the region close to DW domination. The dashed blue contours bound regions where the GW signal is detectable at the design sensitivity of LVK and Einstein Telescope (ET) respectively. The change of slope in the GW regions arises because of an intermediate phase of matter domination driven by the axions produced by the string-wall annihilation. This occurs at small decay temperatures (6), corresponding to the right half of the figure.

Very interestingly, we find that a significant fraction of these GW-observable regions also predicts a detectable nEDM (and/or pEDM) in the near future [32, 68, 69],

i.e. $\Delta\theta \gtrsim 10^{-12}$ ($\Delta\theta \gtrsim 10^{-14}$) (above the dot-dashed and dotted gray contours respectively). Motivated by the exciting possibility of a combined heavy axion discovery via nEDM experiments and GW observatories, we fix $\Delta\theta = 8 \cdot 10^{-13}$ and broaden our analysis to different values of Λ_H in Fig. 2. We find that any $\Lambda_H \gtrsim 10^6$ GeV leads to a GW signal in the foreseen reach of future ground (design LVK, ET, CE) and space based interferometers (LISA [79, 80], DECIGO [81, 82]). The lower right corner in the figure is strongly constrained by the slow decay of axion quanta and a phase of matter domination which spoils BBN. As in Fig. 1, the change of slope in the GW contours is due to an intermediate phase of matter domination, in the lower right part of the figure.

Values of Λ_H smaller than 10^6 GeV can also lead to viable cosmologies, observable GWs and detectable nEDM and/or pEDM, if the potential V_b is temperature-dependent below Λ_H , see Appendix C.

Finally, let us mention that for $\Lambda_H \lesssim 10^{10}$ GeV, LVK are expected to probe the high frequency tail of the GW signal ($\sim \omega^{-1}$), ET can investigate the peak and LISA can probe the low frequency tail ($\sim \omega^3$). Full GW spectra for some representative choices of parameters are shown in Fig. 3.

A caveat is in order before our conclusions: the parameter space shown in Fig. 1 and Fig. 2 is further constrained if V_b arises from dimension-five (and to a less relevant extent from dimension-six) operators with large coefficients. While we discuss this quantitatively in Appendix A, we note here that a large region of parameter space remains unaffected if such operators originate from non-perturbative effects (as can be expected if they are due to gravity, see e.g. [7, 52, 83]).

Conclusions—Heavy QCD axion models can feature

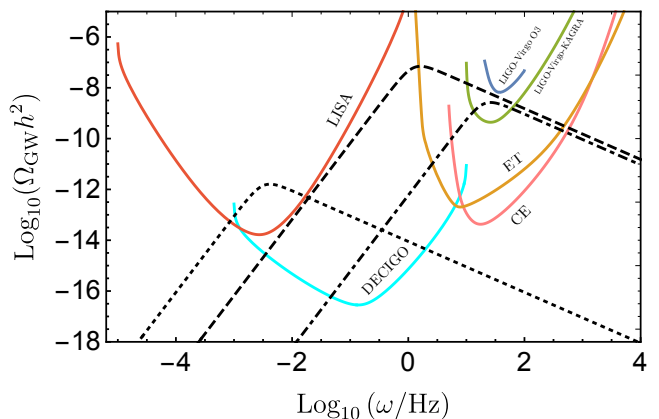


Figure 3. Representative GW spectra (dashed, dotted, dot-dashed lines) for $\kappa_H = 1$ and $N_b = 1, N_{DW} = 6, \delta = 0.3$. Dashed: $\Lambda_H = 10^{10}$ GeV, $f \simeq 3 \cdot 10^{11}$ GeV and $\Delta\theta \simeq 9 \cdot 10^{-11}$. Dotted: $\Lambda_H = 10^7$ GeV, $f = 10^{10}$ GeV $\Delta\theta \simeq 2 \cdot 10^{-12}$. Dot-dashed: $\Lambda_H = 10^{11}$ GeV, $f = 1.6 \cdot 10^{11}$ GeV and $\Delta\theta \simeq 1.2 \cdot 10^{-11}$. Sensitivity curves are taken from [67] and [66] for LIGO-Virgo O3. See also Appendix B.

a long-lived network of topological defects. The main finding of this Letter is that these models predict: i) a stochastic gravitational wave signal measurable by the design LVK interferometers in a large region of parameter space (further broadened by ET and CE, with the possibility of correlated signals also at LISA and DECIGO); ii) a nEDM and/or pEDM measurable in the near future; when: a) the new “heavy QCD” scale is large, i.e. $\Lambda_H \gtrsim 10^{10}$ GeV, thus making the PQ mechanism more robust; and b) misaligned PQ breaking terms that motivate these models in the first place are not strongly suppressed.

Furthermore, we showed that combined GW (at LISA and DECIGO) and nEDM/pEDM signatures also arise for 10^6 GeV $\lesssim \Lambda_H \lesssim 10^{10}$ GeV.

Our results do not strongly depend on the specific heavy QCD axion model, as long as its potential has approximately degenerate minima.

We necessarily left several interesting points for future work. First, in order to precisely characterize the GW signal, numerical simulations of axionic string-wall networks beyond the current literature, possibly including friction and plasma effects, are crucial [64].

Second, we left unspecified the particle content and properties of the “heavy QCD” and of the misaligned PQ breaking sectors. However, these sectors may contain dark matter candidates (see e.g. [84]) or light states that can contribute to the number of extra relativistic degrees of freedom, ΔN_{eff} [85, 86].

Furthermore, it is interesting to understand whether the collapse of the network of topological defects may also lead to a significant fraction of Primordial Black Holes, in a scaled-up version of the mechanism proposed in [87].

Finally, a more complete exploration of the parameter space of heavy axion models may lead to further interesting signatures. For instance, GWs of very low frequency may arise for misaligned sectors lighter than QCD, and may provide a new explanation for recent NANOGrav observations [88]. An investigation of all these aspects is ongoing [89].

Our work is relevant for the ongoing effort to probe well-motivated regions in the parameter space of the PQ mechanism. Guided by the theoretical pursuit of “higher quality” models, we suggest that gravitational wave interferometers and nEDM/pEDM experiments may be the right laboratories to discover the heavy QCD axion.

Acknowledgments—We thank Jaume Garriga, Alex Pomarol and Alex Vilenkin for useful discussions. The work of FR is supported in part by National Science Foundation Grant No. PHY-2013953. The work of RZF and OP was partly supported by the grants FPA2017-88915-P and SEV-2016-0588 from MINECO and 2017-SGR-1069 from DURSI. IFAE is partially funded by the CERCA program of the Generalitat de Catalunya. The work of A.N. is supported by the grants FPA2016-76005-C2-2-P, PID2019-108122GBC32, “Unit of Excellence María de Maeztu 2020-2023” of ICCUB (CEX2019-000918-M), AGAUR2017-SGR-754.

-
- [1] S. Weinberg, *A New Light Boson?*, Phys. Rev. Lett. **40** (1978) 223–226.
- [2] F. Wilczek, *Problem of Strong P and T Invariance in the Presence of Instantons*, Phys. Rev. Lett. **40** (1978) 279–282.
- [3] R. D. Peccei and H. R. Quinn, *CP Conservation in the Presence of Instantons*, Phys. Rev. Lett. **38** (1977) 1440–1443.
- [4] R. D. Peccei and H. R. Quinn, *Constraints Imposed by CP Conservation in the Presence of Instantons*, Phys. Rev. D **16** (1977) 1791–1797.
- [5] H. M. Georgi, L. J. Hall, and M. B. Wise, *Grand Unified Models With an Automatic Peccei-Quinn Symmetry*, Nucl. Phys. B **192** (1981) 409–416.
- [6] B. Holdom and M. E. Peskin, *Raising the Axion Mass*, Nucl. Phys. B **208** (1982) 397–412.
- [7] M. Dine and N. Seiberg, *String Theory and the Strong CP Problem*, Nucl. Phys. B **273** (1986) 109–124.
- [8] R. Holman, S. D. H. Hsu, T. W. Kephart, E. W. Kolb, R. Watkins, and L. M. Widrow, *Solutions to the strong CP problem in a world with gravity*, Phys. Lett. B **282** (1992) 132–136, [[hep-ph/9203206](#)].
- [9] M. Kamionkowski and J. March-Russell, *Planck scale physics and the Peccei-Quinn mechanism*, Phys. Lett. B **282** (1992) 137–141, [[hep-th/9202003](#)].
- [10] S. M. Barr and D. Seckel, *Planck scale corrections to axion models*, Phys. Rev. D **46** (1992) 539–549.
- [11] S. Ghigna, M. Lusignoli, and M. Roncadelli, *Instability of the invisible axion*, Phys. Lett. B **283** (1992) 278–281.
- [12] S. B. Treiman and F. Wilczek, *Axion Emission in Decay of Excited Nuclear States*, Phys. Lett. B **74** (1978) 381–383.
- [13] S. Dimopoulos, *A Solution of the Strong CP Problem in Models With Scalars*, Phys. Lett. B **84** (1979) 435–439.
- [14] S. H. H. Tye, *A Superstrong Force With a Heavy Axion*, Phys. Rev. Lett. **47** (1981) 1035.
- [15] B. Holdom, *Strong QCD at High-energies and a Heavy Axion*, Phys. Lett. B **154** (1985) 316. [Erratum: Phys.Lett.B 156, 452 (1985)].
- [16] J. M. Flynn and L. Randall, *A Computation of the Small Instanton Contribution to the Axion Potential*, Nucl. Phys. B **293** (1987) 731–739.
- [17] K. Choi and H. D. Kim, *Small instanton contribution to the axion potential in supersymmetric models*, Phys. Rev. D **59** (1999) 072001, [[hep-ph/9809286](#)].
- [18] P. Agrawal and K. Howe, *Factoring the Strong CP Problem*, JHEP **12** (2018) 029, [[arXiv:1710.04213](#)].
- [19] R. Kitano and W. Yin, *Strong CP problem and axion dark matter with small instantons*, JHEP **07** (2021) 078, [[arXiv:2103.08598](#)].
- [20] T. Gherghetta, V. V. Khoze, A. Pomarol, and Y. Shirman, *The Axion Mass from 5D Small Instantons*, JHEP **03** (2020) 063, [[arXiv:2001.05610](#)].
- [21] V. A. Rubakov, *Grand unification and heavy axion*, JETP Lett. **65** (1997) 621–624, [[hep-ph/9703409](#)].
- [22] T. Gherghetta, N. Nagata, and M. Shifman, *A Visible*

- QCD Axion from an Enlarged Color Group*, Phys. Rev. D **93** (2016), no. 11 115010, [arXiv:1604.01127].
- [23] T. Gherghetta and M. D. Nguyen, *A Composite Higgs with a Heavy Composite Axion*, JHEP **12** (2020) 094, [arXiv:2007.10875].
- [24] Z. Berezhiani, L. Gianfagna, and M. Giannotti, *Strong CP problem and mirror world: The Weinberg-Wilczek axion revisited*, Phys. Lett. B **500** (2001) 286–296, [hep-ph/0009290].
- [25] S. Dimopoulos, A. Hook, J. Huang, and G. Marques-Tavares, *A collider observable QCD axion*, JHEP **11** (2016) 052, [arXiv:1606.03097].
- [26] A. Hook, S. Kumar, Z. Liu, and R. Sundrum, *High Quality QCD Axion and the LHC*, Phys. Rev. Lett. **124** (2020), no. 22 221801, [arXiv:1911.12364].
- [27] M. Bauer, M. Heiles, M. Neubert, and A. Thamm, *Axion-Like Particles at Future Colliders*, Eur. Phys. J. C **79** (2019), no. 1 74, [arXiv:1808.10323].
- [28] S. Chakraborty, M. Kraus, V. Loladze, T. Okui, and K. Tobioka, *Heavy QCD Axion in $b \rightarrow s$ transition: Enhanced Limits and Projections*, arXiv:2102.04474.
- [29] **LIGO Scientific** Collaboration, J. Aasi et. al., *Advanced LIGO*, Class. Quant. Grav. **32** (2015) 074001, [arXiv:1411.4547].
- [30] **VIRGO** Collaboration, F. Acernese et. al., *Advanced Virgo: a second-generation interferometric gravitational wave detector*, Class. Quant. Grav. **32** (2015), no. 2 024001, [arXiv:1408.3978].
- [31] **KAGRA** Collaboration, T. Akutsu et. al., *KAGRA: 2.5 Generation Interferometric Gravitational Wave Detector*, Nature Astron. **3** (2019), no. 1 35–40, [arXiv:1811.08079].
- [32] C. Abel et. al., *The $n2EDM$ experiment at the Paul Scherrer Institute*, EPJ Web Conf. **219** (2019) 02002, [arXiv:1811.02340].
- [33] B. W. Filippone, *Worldwide Search for the Neutron EDM*, 13th Conference on the Intersections of Particle and Nuclear Physics (10, 2018) [arXiv:1810.03718].
- [34] X. Martin and A. Vilenkin, *Gravitational wave background from hybrid topological defects*, Phys. Rev. Lett. **77** (1996) 2879–2882, [astro-ph/9606022].
- [35] A. Vilenkin and A. E. Everett, *Cosmic Strings and Domain Walls in Models with Goldstone and PseudoGoldstone Bosons*, Phys. Rev. Lett. **48** (1982) 1867–1870.
- [36] P. Sikivie, *Of Axions, Domain Walls and the Early Universe*, Phys. Rev. Lett. **48** (1982) 1156–1159.
- [37] T. Hiramatsu, M. Kawasaki, K. Saikawa, and T. Sekiguchi, *Axion cosmology with long-lived domain walls*, JCAP **01** (2013) 001, [arXiv:1207.3166].
- [38] M. Dine, W. Fischler, and M. Srednicki, *A Simple Solution to the Strong CP Problem with a Harmless Axion*, Phys. Lett. B **104** (1981) 199–202.
- [39] A. R. Zhitnitsky, *On Possible Suppression of the Axion Hadron Interactions. (In Russian)*, Sov. J. Nucl. Phys. **31** (1980) 260.
- [40] J. E. Kim, *Weak Interaction Singlet and Strong CP Invariance*, Phys. Rev. Lett. **43** (1979) 103.
- [41] M. A. Shifman, A. I. Vainshtein, and V. I. Zakharov, *Can Confinement Ensure Natural CP Invariance of Strong Interactions?*, Nucl. Phys. B **166** (1980) 493–506.
- [42] B. Holdom, *DOMAIN WALLS. 1. AXION MODELS*, Phys. Rev. D **27** (1983) 332–338.
- [43] B. Von Harling, A. Pomarol, O. Pujolàs, and F. Rompineve, *Peccei-Quinn Phase Transition at LIGO*, JHEP **04** (2020) 195, [arXiv:1912.07587].
- [44] L. Delle Rose, G. Panico, M. Redi, and A. Tesi, *Gravitational Waves from Supercool Axions*, JHEP **04** (2020) 025, [arXiv:1912.06139].
- [45] N. Ramberg and L. Visinelli, *Probing the Early Universe with Axion Physics and Gravitational Waves*, Phys. Rev. D **99** (2019), no. 12 123513, [arXiv:1904.05707].
- [46] N. Ramberg and L. Visinelli, *QCD axion and gravitational waves in light of NANOGrav results*, Phys. Rev. D **103** (2021), no. 6 063031, [arXiv:2012.06882].
- [47] R. Daido, N. Kitajima, and F. Takahashi, *Axion domain wall baryogenesis*, JCAP **07** (2015) 046, [arXiv:1504.07917].
- [48] T. Higaki, K. S. Jeong, N. Kitajima, T. Sekiguchi, and F. Takahashi, *Topological Defects and nano-Hz Gravitational Waves in Aligned Axion Models*, JHEP **08** (2016) 044, [arXiv:1606.05552].
- [49] C.-W. Chiang and B.-Q. Lu, *Testing clockwork axion with gravitational waves*, JCAP **05** (2021) 049, [arXiv:2012.14071].
- [50] G. B. Gelmini, A. Simpson, and E. Vitagliano, *Gravitational waves from axionlike particle cosmic string-wall networks*, Phys. Rev. D **104** (2021), no. 6 061301, [arXiv:2103.07625].
- [51] G. Dvali, *Three-form gauging of axion symmetries and gravity*, hep-th/0507215.
- [52] P. Svrcek and E. Witten, *Axions In String Theory*, JHEP **06** (2006) 051, [hep-th/0605206].
- [53] A. Hebecker, T. Mikhail, and P. Soler, *Euclidean wormholes, baby universes, and their impact on particle physics and cosmology*, Front. Astron. Space Sci. **5** (2018) 35, [arXiv:1807.00824].
- [54] **nEDM** Collaboration, C. Abel et. al., *Measurement of the permanent electric dipole moment of the neutron*, Phys. Rev. Lett. **124** (2020), no. 8 081803, [arXiv:2001.11966].
- [55] S. Borsanyi et. al., *Calculation of the axion mass based on high-temperature lattice quantum chromodynamics*, Nature **539** (2016), no. 7627 69–71, [arXiv:1606.07494].
- [56] T. W. B. Kibble, *Topology of Cosmic Domains and Strings*, J. Phys. A **9** (1976) 1387–1398.
- [57] T. W. B. Kibble, *Some Implications of a Cosmological Phase Transition*, Phys. Rept. **67** (1980) 183.
- [58] A. Vilenkin and E. P. S. Shellard, *Cosmic Strings and Other Topological Defects*. Cambridge University Press, 7, 2000.
- [59] M. Gorghetto, E. Hardy, and G. Villadoro, *Axions from Strings: the Attractive Solution*, JHEP **07** (2018) 151, [arXiv:1806.04677].
- [60] M. Hindmarsh, J. Lizarraga, A. Lopez-Eiguren, and J. Urrestilla, *Scaling Density of Axion Strings*, Phys. Rev. Lett. **124** (2020), no. 2 021301, [arXiv:1908.03522].
- [61] M. Gorghetto, E. Hardy, and G. Villadoro, *More Axions from Strings*, SciPost Phys. **10** (2021) 050, [arXiv:2007.04990].
- [62] M. Hindmarsh, J. Lizarraga, A. Lopez-Eiguren, and J. Urrestilla, *Approach to scaling in axion string networks*, Phys. Rev. D **103** (2021), no. 10 103534, [arXiv:2102.07723].
- [63] Y. B. Zeldovich, I. Y. Kobzarev, and L. B. Okun, *Cosmological Consequences of the Spontaneous*

- Breakdown of Discrete Symmetry*, Zh. Eksp. Teor. Fiz. **67** (1974) 3–11.
- [64] M. Kawasaki, K. Saikawa, and T. Sekiguchi, *Axion dark matter from topological defects*, Phys. Rev. D **91** (2015), no. 6 065014, [[arXiv:1412.0789](#)].
- [65] D. Aloni, Y. Soreq, and M. Williams, *Coupling QCD-Scale Axionlike Particles to Gluons*, Phys. Rev. Lett. **123** (2019), no. 3 031803, [[arXiv:1811.03474](#)].
- [66] **LIGO Scientific, Virgo, KAGRA** Collaboration, R. Abbott et. al., *Upper Limits on the Isotropic Gravitational-Wave Background from Advanced LIGO's and Advanced Virgo's Third Observing Run*, [arXiv:2101.12130](#).
- [67] K. Schmitz, *New Sensitivity Curves for Gravitational-Wave Signals from Cosmological Phase Transitions*, JHEP **01** (2021) 097, [[arXiv:2002.04615](#)].
- [68] **nEDM** Collaboration, M. W. Ahmed et. al., *A New Cryogenic Apparatus to Search for the Neutron Electric Dipole Moment*, JINST **14** (2019), no. 11 P11017, [[arXiv:1908.09937](#)].
- [69] Z. Omarov, H. Davoudiasl, S. Hacımeroglu, V. Lebedev, W. M. Morse, Y. K. Semertzidis, A. J. Silenko, E. J. Stephenson, and R. Suleiman, *Comprehensive Symmetric-Hybrid ring design for pEDM experiment at below 10^{-29} e-cm*, [arXiv:2007.10332](#).
- [70] A. Vilenkin, *Gravitational Field of Vacuum Domain Walls and Strings*, Phys. Rev. D **23** (1981) 852–857.
- [71] J. Preskill, S. P. Trivedi, F. Wilczek, and M. B. Wise, *Cosmology and broken discrete symmetry*, Nucl. Phys. B **363** (1991) 207–220.
- [72] S. Chang, C. Hagmann, and P. Sikivie, *Studies of the motion and decay of axion walls bounded by strings*, Phys. Rev. D **59** (1999) 023505, [[hep-ph/9807374](#)].
- [73] M. Gleiser and R. Roberts, *Gravitational waves from collapsing vacuum domains*, Phys. Rev. Lett. **81** (1998) 5497–5500, [[astro-ph/9807260](#)].
- [74] T. Hiramatsu, M. Kawasaki, and K. Saikawa, *Gravitational Waves from Collapsing Domain Walls*, JCAP **05** (2010) 032, [[arXiv:1002.1555](#)].
- [75] M. Kawasaki and K. Saikawa, *Study of gravitational radiation from cosmic domain walls*, JCAP **09** (2011) 008, [[arXiv:1102.5628](#)].
- [76] T. Hiramatsu, M. Kawasaki, and K. Saikawa, *On the estimation of gravitational wave spectrum from cosmic domain walls*, JCAP **02** (2014) 031, [[arXiv:1309.5001](#)].
- [77] **LIGO Scientific** Collaboration, L. Barsotti, P. Fritschel, M. Evans, and G. Slawomir, *Updated Advanced LIGO sensitivity design curve*, . <https://dcc.ligo.org/LIGO-T1800044/public>.
- [78] **LIGO Scientific** Collaboration, C. Berry, B. O'Reilly, M. Razzano, S. Fairhurst, and P. Sutton, *Updated Advanced LIGO sensitivity design curve*, . <https://dcc.ligo.org/LIGO-P1200087-v47/public>.
- [79] **LISA** Collaboration, P. Amaro-Seoane et. al., *Laser Interferometer Space Antenna*, arXiv e-prints (Feb., 2017) arXiv:1702.00786, [[arXiv:1702.00786](#)].
- [80] J. Baker et. al., *The Laser Interferometer Space Antenna: Unveiling the Millihertz Gravitational Wave Sky*, [arXiv:1907.06482](#).
- [81] K. Yagi and N. Seto, *Detector configuration of DECIGO/BBO and identification of cosmological neutron-star binaries*, Phys. Rev. D **83** (2011) 044011, [[arXiv:1101.3940](#)]. [Erratum: Phys.Rev.D 95, 109901 (2017)].
- [82] S. Isoyama, H. Nakano, and T. Nakamura, *Multiband Gravitational-Wave Astronomy: Observing binary inspirals with a decihertz detector, B-DECIGO*, PTEP **2018** (2018), no. 7 073E01, [[arXiv:1802.06977](#)].
- [83] R. Kallosh, A. D. Linde, D. A. Linde, and L. Susskind, *Gravity and global symmetries*, Phys. Rev. D **52** (1995) 912–935, [[hep-th/9502069](#)].
- [84] R. Garani, M. Redi, and A. Tesi, *Dark QCD Matters*, [arXiv:2105.03429](#).
- [85] **Planck** Collaboration, N. Aghanim et. al., *Planck 2018 results. VI. Cosmological parameters*, Astron. Astrophys. **641** (2020) A6, [[arXiv:1807.06209](#)].
- [86] **CMB-S4** Collaboration, K. N. Abazajian et. al., *CMB-S4 Science Book, First Edition*, [arXiv:1610.02743](#).
- [87] F. Ferrer, E. Mazzo, G. Panico, O. Pujolas, and F. Rompineve, *Primordial Black Holes from the QCD axion*, Phys. Rev. Lett. **122** (2019), no. 10 101301, [[arXiv:1807.01707](#)].
- [88] **NANOGrav** Collaboration, Z. Arzoumanian et. al., *The NANOGrav 12.5 yr Data Set: Search for an Isotropic Stochastic Gravitational-wave Background*, Astrophys. J. Lett. **905** (2020), no. 2 L34, [[arXiv:2009.04496](#)].
- [89] R. Z. Ferreira, A. Notari, O. Pujolas, and F. Rompineve, *in preparation*, .
- [90] T. Banks and M. Dine, *The Cosmology of string theoretic axions*, Nucl. Phys. B **505** (1997) 445–460, [[hep-th/9608197](#)].
- [91] L. Hui, J. P. Ostriker, S. Tremaine, and E. Witten, *Ultralight scalars as cosmological dark matter*, Phys. Rev. D **95** (2017), no. 4 043541, [[arXiv:1610.08297](#)].
- [92] D. J. Gross, R. D. Pisarski, and L. G. Yaffe, *QCD and Instantons at Finite Temperature*, Rev. Mod. Phys. **53** (1981) 43.
- [93] **Particle Data Group** Collaboration, P. Zyla et. al., *Review of Particle Physics*, PTEP **2020** (2020), no. 8 083C01.
- [94] A. E. Everett, *Observational consequences of a 'domain' structure of the universe*, Phys. Rev. D **10** (1974) 3161–3166.
- [95] K. Nakayama, F. Takahashi, and N. Yokozaki, *Gravitational waves from domain walls and their implications*, Phys. Lett. B **770** (2017) 500–506, [[arXiv:1612.08327](#)].

Appendix A: Origin of misaligned contributions

In this section, we critically review well-motivated origins for misaligned contributions of the form

$$V_b \simeq -\mu_b^4 \cos\left(\frac{N_b}{N_{\text{DW}}} \frac{a}{f} - \delta\right). \quad (\text{A1})$$

Such contributions can be generated at a scale Λ_b such that $\mu_b = \kappa_b^{1/2} \Lambda_b$, with $\kappa_b \leq 1$.

Let us first consider misaligned terms generated at $\Lambda_b \gg f \gg \Lambda_H$. The following possibilities can then be envisioned:

1 - Non-perturbative corrections to the axion potential, among them: stringy and/or gravitational

instantons, in which case $\kappa_b \sim e^{-S/2}$, where S is the instanton action of interest (see e.g. the discussions in [52] for stringy instantons and [53] for gravitational instantons); instantons of another gauge sector with confinement scale Λ_b and a light fermion of mass m_q , giving $\kappa_b \sim (m_q/\Lambda_b)^{1/2}$.

2 - Higher-dimensional operators \mathcal{O}_Δ inducing

$$V_b \sim c_\Delta \frac{\mathcal{O}_\Delta(\Phi)}{\Lambda_b^{\Delta-4}} + \text{h.c.}, \quad (\text{A2})$$

with $\Delta > 4$ in scenarios where the axion is the phase of a complex scalar field Φ , whose renormalizable Lagrangian respects the PQ symmetry, giving $\kappa_b \sim \sqrt{c_\Delta}(N_{\text{DW}}f/\Lambda_b)^{\Delta/2}$. The size of the coefficients c_Δ depends on the specific origin of the higher dimensional operators.

The contributions above are often discussed as a source of the quality problem, since they induce the shift of the QCD vacuum angle given in eq. (4) of the main text and reported here for the reader's convenience: $\Delta\theta \simeq r^4(N_b/N_{\text{DW}})(\sin\delta/\kappa_H)$, with $r \equiv \mu_b/\Lambda_H$. Imposing that the QCD axion solution to the strong CP problem is kept, the following constraints on the two contributions above arise:

1 - For contributions with $\kappa_b \sim e^{-S/2}$, one finds:

$$S \gtrsim 76 + 4 \log\left(\frac{\Lambda_b}{10^{16} \text{ GeV}}\right) - 4 \log\left(\frac{\Lambda_H}{10^{10} \text{ GeV}}\right) - \log\left(\frac{\theta}{10^{-10}}\right) + \log\left(\frac{\sin\delta}{\kappa_H^2}\right), \quad (\text{A3})$$

whereas for contributions from confining gauge sectors with $\kappa_b \sim (m_q/\Lambda_b)^{1/2}$, one finds the following constraint on the light fermion mass:

$$\frac{m_q}{\Lambda_b} \lesssim 10^{-10} \left(\frac{N_{\text{DW}}}{N_b}\right) \left(\frac{\kappa_H^2}{\sin\delta}\right) \left(\frac{\Lambda_H}{\Lambda_b}\right)^4 \left(\frac{\theta}{10^{-10}}\right). \quad (\text{A4})$$

In both cases, it is evident that taking Λ_H as large as possible provides the most robust implementation of the PQ mechanism. In particular, the lower bound on the instanton action (A3) is reduced by approximately a factor of two for $\Lambda_H \simeq 10^{10}$ GeV with respect to the standard QCD axion. This can importantly relax the quality problem in certain setups [7].

2 - For contributions with $\kappa_b \sim \sqrt{c_\Delta}(N_{\text{DW}}f/\Lambda_b)^{\Delta/2}$, one finds, focusing on the most important operators, i.e.

those of dimension $\Delta = 5, 6$:

$$\Lambda_H \gtrsim 5 \text{ TeV} \left(\frac{N_{\text{DW}}}{6}\right) \left(\frac{c_5}{\kappa_H^2}\right)^{\frac{1}{4}} \left(\frac{f}{10^4 \text{ GeV}}\right)^{5/4} \times \left(\frac{10^{19} \text{ GeV}}{\Lambda_b}\right)^{\frac{1}{4}} \left(\frac{10^{-10}}{\theta}\right)^{\frac{1}{4}}, \quad \text{for } \Delta = 5, \quad (\text{A5})$$

$$\Lambda_H \gtrsim 10^9 \text{ GeV} \left(\frac{N_{\text{DW}}}{6}\right)^{\frac{5}{4}} \left(\frac{c_6}{\kappa_H^2}\right)^{\frac{1}{4}} \left(\frac{f}{10^{10} \text{ GeV}}\right)^{3/2} \times \left(\frac{10^{19} \text{ GeV}}{\Lambda_b}\right)^{\frac{1}{2}} \left(\frac{10^{-10}}{\theta}\right)^{\frac{1}{4}}, \quad \text{for } \Delta = 6. \quad (\text{A6})$$

The lower bounds above should be complemented with the upper bound $\Lambda_H \leq f$, which arises from consistency of the axion EFT. We have normalized Λ_b to the Planck scale, to reflect the common assumption in the literature that the operators \mathcal{O}_Δ may be induced by gravitational interactions, see e.g. [9].

The relevance of these constraints depends crucially on the size of the coefficients c_Δ . It is sometimes assumed that $c_\Delta \sim O(1)$, which may be justified if UV physics, in particular gravity, breaks the PQ symmetry perturbatively. Under this assumption, (A5) imposes a very stringent constraint on Λ_H , which can be satisfied only for $5 \text{ TeV} \lesssim \Lambda_H \lesssim f \sim 10 \text{ TeV}$. This would severely limit the interesting region of the parameter space shown in Figs. 1 and 2 of our main text.

On the other hand, arguments against global symmetries in gravitational theories suggest that the latter may break the PQ symmetry only via non-perturbative effects (see e.g. [7, 52, 83, 90]). In this case, higher dimensional operators may still be generated, albeit the coefficients c_Δ would then be expected to be exponentially suppressed by the corresponding instanton action, as in case 1 above. Typical values $S_{\text{inst}} \sim O(100)$ (see e.g. [52, 91]) render Planck-suppressed operators irrelevant for the heavy QCD axion scenario considered in this work. Nonetheless, we may consider much smaller values of the action (as suggested by) to understand what suppression would be required to affect our parameter space, as we do in Fig. 4 (left) for dimension $\Delta = 5$ operators and $\kappa_H = 1$. We note that even for $c_5 \lesssim 10^{-7}$, corresponding to a very small instanton action $S_{\text{inst}} \simeq 15$ (this roughly coincides with $S_{\text{inst}} \sim \ln M_p/f$ for $f \gtrsim 10^{11}$ GeV, which is the smallest estimate of the action from non-perturbative gravitational contributions [83]), there exists a region of available parameter space where the GW signal is detectable at LIGO-Virgo-KAGRA (LVK), and that for $c_5 \lesssim 10^{-15}$, corresponding to $S_{\text{inst}} \simeq 34$ the LVK region is entirely available.

It is also conceivable that dimension-5 operators may be forbidden in a concrete model. In this case, the most dangerous operators would be those of dimension 6. Constraints from (A6) are shown in Fig. 4 (right). We note that in this case even the choice $c_6 \sim 1$ leaves an available region of parameter space which overlaps with

the LVK reach, and that for $c_6 \sim 10^{-7}$ the entire region is available.

This is dramatically different from the situation in the standard (light) QCD axion case, where all operators up to dimension 9 (or 12 depending on the value of f) have to be forbidden in order for the axion to solve the strong CP problem.

Scenarios with $\Lambda_b \ll \Lambda_H$ can also arise from a confining gauge sector. Then $\kappa_b \sim (m_q/\Lambda_b)^{1/2}$ as in case **1** above. The quality problem in this case can then be evaded by taking Λ_b sufficiently below Λ_H . Nonetheless, in contrast to the heavy QCD axion case, this is difficult in the standard QCD axion case where Λ_b is bounded from below by the overproduction of axion dark matter from the decay of the axion string-wall network (see e.g. [87]).

Appendix B: Network Evolution

Here we report full formulae for quantities defined in the main text, including the dependence on all parameters. We start with the temperature-dependent axion mass $m_{a,H}$. We used the parametrization

$$\begin{aligned} m_a(T) &= m_a \left(\frac{T_{0,H}}{T} \right)^\gamma, \quad \text{for } T \geq T_{0,H} \\ m_a(T) &= \kappa_H \frac{\Lambda_H^2}{f}, \quad \text{for } T < T_{0,H} \end{aligned} \quad (\text{B1})$$

where $T_{0,H}$ is a critical temperature, analogous to the critical temperature in QCD. Usually, $T_{0,H} \lesssim \Lambda_H$, for instance in QCD $T_0 \simeq 134 \text{ MeV} \simeq 0.4 \Lambda_{\text{QCD}}$ [55]. The exponent γ can be estimated analytically at $T \gg \Lambda_H$ in the Dilute Instanton Gas Approximation (DIGA). For $G = SU(N_c)$ with N_f light flavors, one finds [92]: $\gamma \simeq 11N_c/6 + N_f/6 - 2$. Lattice calculations are required to compute γ at $T \gtrsim \Lambda_H$. However, in the case of QCD, available lattice results agree well with the DIGA estimate [55]. In order to produce the blue shaded region in our figures, we have fixed $\gamma = 4, T_{0,H} = \Lambda_H$.

The parameter κ_H suppresses the heavy axion mass in models where G contains at least one light fermion ψ , in which case $\kappa_H = \sqrt{m_\psi}/\Lambda_H$. Alternatively, κ_H can also be much smaller than unity in models where m_a arises from *small instantons* of QCD itself, when the latter becomes strongly coupled in the UV, above the EW phase transition [6, 15–17, 20]. In this case SM quarks are massless and κ_H is proportional to powers of their Yukawa couplings, see e.g. [20].

The temperature at which the heavy axion starts its oscillations is determined by imposing the condition $3H = m_a(T)$:

$$\begin{aligned} T_{\text{osc}} &\simeq c_\gamma \cdot 10^{11} \text{ GeV} \kappa_H^{\frac{1}{2+n}} \left(\frac{106.75}{g_*(T_{\text{osc}})} \right)^{\frac{1}{4+2n}} \\ &\times \left(\frac{\Lambda}{10^{10} \text{ GeV}} \right) \left(\frac{10^{12} \text{ GeV}}{f} \right)^{\frac{1}{2+n}}. \end{aligned} \quad (\text{B2})$$

where c_γ varies by a $O(1)$ factor with γ . For $\gamma = 4$ and $f = 10^{12} \text{ GeV}$, one finds $T_{\text{osc}} \simeq 10^{11} \text{ GeV}$. For certain values of $f, r \equiv \mu_b/\Lambda_H$ and Λ_H , the heavy axion starts oscillating in the potential V_b at temperatures above (B2). Obviously, this can only happen if V_b is larger than V_a at high temperatures, for instance when V_b is temperature-independent at temperatures slightly above Λ_H (the temperature-dependent case is discussed in Appendix C). In this case, the temperature at which the axion would start oscillating around one of the minima of V_b is given by

$$\begin{aligned} T_{\text{osc}, b} &\simeq 5 \cdot 10^9 \text{ GeV} \left(\frac{\mu_b}{10^7 \text{ GeV}} \right) \left(\frac{N_b}{N_{\text{DW}}} \right)^{\frac{1}{2}} \\ &\times \left(\frac{106.75}{g_*(T_{\text{osc}, b})} \right)^{\frac{1}{4}} \left(\frac{10^{12} \text{ GeV}}{f} \right)^{\frac{1}{2}}. \end{aligned} \quad (\text{B3})$$

In this case the scenario may still be cosmologically viable (if it satisfies other constraints), but the first domain walls to form are those of V_b , rather than of V_a . Their tension is significantly smaller than that of the V_a walls, since $r \ll 1$. Furthermore, if $N_b = 1$, then the V_b network annihilates at high temperatures and there are no walls formed at T_{osc} . If N_b is co-prime with N_{DW} , annihilation occurs close to Λ_H . Thus in this case the gravitational wave signal is suppressed compared to the case analyzed in the main text. However, we find that this occurs only in a tiny region of the parameter space, located in the upper left corner of Fig. 1 of the main text.

When $T_{\text{osc}, b} \ll T_{\text{osc}}$, the network forms as described in the text. We assume that it quickly reaches the scaling regime, where $\rho_{\text{dw}} = c\sigma H(T)$. The annihilation temperature is then found by imposing the condition $d\sigma H = \Delta V$, where d is a numerical parameter. One finds:

$$\begin{aligned} T_{\text{ann}} &\simeq 10^8 \text{ GeV} \frac{\sin(N_b\pi/N_{\text{DW}})}{\sqrt{c} d \sqrt{\kappa_H}} \left(\frac{106.75}{g_{\text{ann}}} \right)^{\frac{1}{4}} \\ &\times \left(\frac{10^{12} \text{ GeV}}{f} \right)^{\frac{1}{2}} \left(\frac{\Lambda_H}{10^{10} \text{ GeV}} \right) \left(\frac{r}{0.005} \right)^2, \end{aligned} \quad (\text{B4})$$

where we kept the explicit dependence on all parameters, while in the text we fixed $N_b = 1, N_{\text{DW}} = 6, \kappa_H = 1$ as representative example. The parameters c and d are determined by numerical simulations [64] and depend on N_{DW} (and presumably N_b). The relations to the parameters extracted from numerical simulations in [64] are $c = 2\mathcal{A}, d = 2C_d$. For instance, for our example choice $N_{\text{DW}} = 6$ the numerical simulations of [64] find central values $\mathcal{A} = 2.24, C_d = 3.14$ (we follow the 1% criterion in [64]), so that $c = 4.48, d = 6.28$.

The string-wall network may dominate the energy density of the Universe, if annihilation is too slow. The temperature corresponding to network domination is

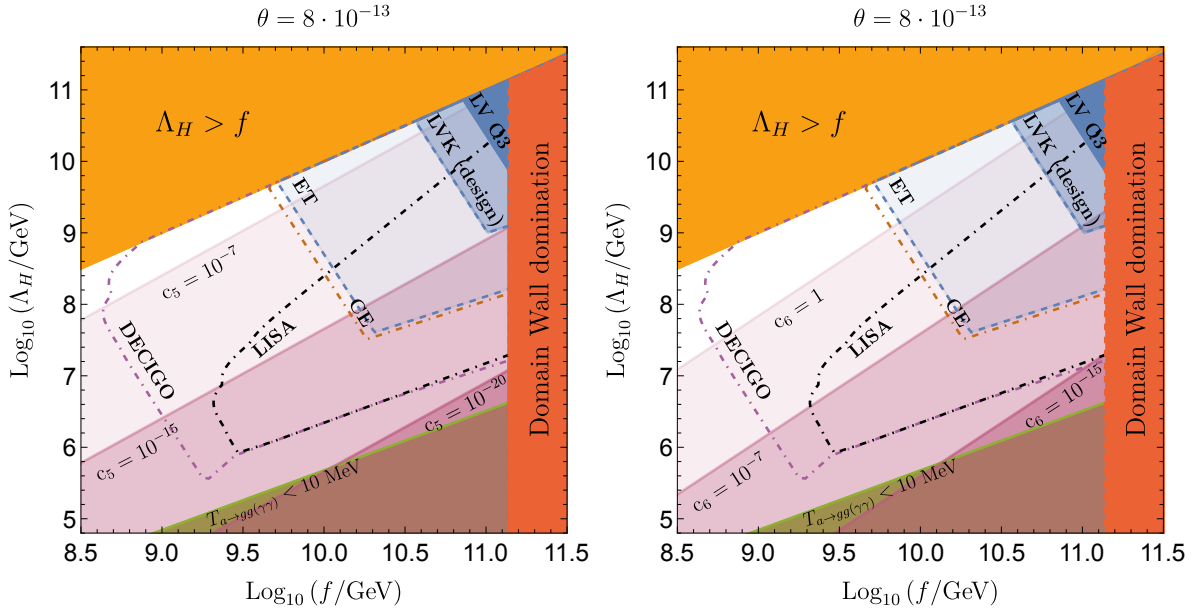


Figure 4. *Left*: Same as Fig. 2 of the main text, with the constraint (A5) for several choices of c_5 and with $\kappa_H = 1$, under the assumption that Planck-suppressed dimension-5 operators which break the PQ symmetry are present. *Right*: same as the left figure, for dimension-6 operators.

estimated by imposing $c\sigma H = 3H^2 M_p^2$.

$$T_{\text{dw-dom}} \simeq 6 \cdot 10^6 \text{ GeV} \sqrt{c\kappa_H} \left(\frac{106.75}{g_{*,\text{dw-dom}}} \right)^{\frac{1}{4}} \times \left(\frac{f}{10^{12} \text{ GeV}} \right)^{\frac{1}{2}} \left(\frac{\Lambda_H}{10^{10} \text{ GeV}} \right). \quad (\text{B5})$$

In the shaded regions denoted with “DW domination” in Figures 1 and 2 in the main text, $T_{\text{dw-dom}} > T_{\text{ann}}$. In this case it is in general problematic to gracefully exit the domain wall dominated phase, at least in the axion scenario considered in this work.

The heavy axion decay rate into SM gluons (photons) is given by:

$$\Gamma_{a \rightarrow gg(\gamma\gamma)} = \frac{1}{64\pi} \left(\frac{c_g(\gamma)\alpha_s(\text{em})}{2\pi} \right)^2 \frac{m_a^3}{f^2}, \quad (\text{B6})$$

where $c_g = 1$ and $c_\gamma = E/N_{\text{DW}} - 1.92$, with E being the model-dependent electromagnetic anomaly (see e.g. [93] for a review in standard DFSZ and KSVZ constructions) and the -1.92 arising only below the QCD PT. The decay is efficient once $\Gamma \simeq H$, which gives:

$$T_{a \rightarrow gg(\gamma\gamma)} \simeq 9 \cdot 10^6 \text{ GeV} \alpha_{s(\text{EM})} \kappa_H^{3/2} \times \left(\frac{\Lambda_H}{10^{10} \text{ GeV}} \right)^3 \left(\frac{10^{12} \text{ GeV}}{f} \right)^{\frac{5}{2}} \quad (\text{B7})$$

In models where $E/N \neq 0$, the decay channel to photons is in principle available above the EWPT, but it is less efficient than the channel to gluons (we use $\alpha_s = 0.1$ in

our Figures). Below the QCD PT, the latter remains available when $m_a \gtrsim 1 \text{ GeV}$ [65], which happens in most of the parameter space of interest, otherwise the decay temperature should be computed according to the $a \rightarrow \gamma\gamma$ rate. In the shaded blue region denoted by “Life-Time” in Fig. 2 of the main text the decay temperature is below 10 MeV. In this case products of axion decay can be dangerous for BBN. When the decay temperatures above are larger than the annihilation temperature of the network, the latter rapidly transfers its energy to the SM at T_{ann} .

The annihilation of the string-wall network leads to a population of mildly relativistic axions, which soon contributes to the dark matter abundance. When the decay rates (B6) are not fast enough, these axions can dominate the energy density of the Universe and lead to a temporary phase of matter domination. The temperature at which the matter dominated phase starts is found by imposing

$$c\sigma H(T_{\text{ann}}) \left(\frac{g_*(T)}{g_{*,\text{ann}}} \right) \left(\frac{T}{T_{\text{ann}}} \right)^3 = 3H(T)M_p^2$$

which gives

$$T_{\text{MD}} = 8 \cdot 10^6 \text{ GeV} \left(\frac{\sqrt{d}(c\kappa_H)^{3/2}}{\sin(N_b\pi/N_{\text{DW}})} \right) \left(\frac{106.75}{g_{*,\text{ann}}} \right)^{\frac{1}{4}} \times \left(\frac{f}{10^{12} \text{ GeV}} \right)^{\frac{3}{2}} \left(\frac{\Lambda_H}{10^{10} \text{ GeV}} \right) \left(\frac{0.001}{r} \right)^2. \quad (\text{B8})$$

The temperature above should be compared with the decay temperatures (B7): whenever the former is

larger, there is a phase of matter domination which should be taken into account when computing the gravitational wave signal. In principle, cold axions from the misalignment mechanism may also lead to an intermediate phase of matter domination. However, we find that in the regions of parameter space shown in the Figures, their contribution is subdominant compared to the axions from string-wall annihilation.

Let us finally provide formulae for the gravitational wave signal. The peak frequency of the signal at the time of network annihilation is approximately given by the Hubble rate at that epoch, i.e. $\omega_{\text{peak}} \simeq H(T_{\text{ann}})$. Let us first consider the case in which the Universe is radiation dominated after domain wall annihilation. The redshifted frequency is then given by

$$\omega_{\text{peak}} \simeq 56 \text{ Hz} \frac{\sin(N_b \pi / N_{\text{DW}})}{\sqrt{\kappa_{\text{HC}} d}} \left(\frac{r}{0.005} \right)^2 \times \left(\frac{106.75}{g_{*,\text{ann}}} \right)^{\frac{1}{2}} \left(\frac{\Lambda_{\text{H}}}{10^{10} \text{ GeV}} \right) \left(\frac{10^{11} \text{ GeV}}{f} \right)^{\frac{1}{2}}. \quad (\text{B9})$$

where, as mentioned in the main text, we have assumed $g_{*,\text{ann}} = g_{s,\text{ann}}$ throughout the work. The amplitude of the signal at the peak frequency is instead given explicitly by [76]

$$\Omega_{\text{gw}} h^2 \simeq 0.01 (\Omega_{\gamma} h^2) \tilde{\epsilon} \left(\frac{106.75}{g_{*,\text{ann}}} \right)^{\frac{1}{3}} \left(\frac{\rho_{\text{dw}}}{\rho_{\text{rel}}} \right)_{T=T_{\text{ann}}}^2 \simeq 6 \cdot 10^{-9} \frac{c^4 d^2 \tilde{\epsilon} \kappa_{\text{H}}^4}{\sin(N_b \pi / N_{\text{DW}})^4} \left(\frac{106.75}{g_{*,\text{ann}}} \right)^{\frac{1}{3}} \times \left(\frac{f}{10^{12} \text{ GeV}} \right)^4 \left(\frac{0.002}{r} \right)^8, \quad (\text{B10})$$

where $\Omega_{\gamma} h^2 \simeq 4 \cdot 10^{-5}$ is the relic abundance of radiation today and $\tilde{\epsilon}$ is a numerical prefactor taken from simulations and of order 0.1–1 [37]. To produce the plots we used $\tilde{\epsilon} = 0.7$.

In the presence of an intermediate phase of matter domination, the formulae above should be adjusted to take into account the different redshift. In particular:

$$\omega_{\text{peak, MD}} \simeq H(T_{\text{ann}}) \left(\frac{a(T_{\text{ann}})}{a(T_{\text{MD}})} \right) \times \left(\frac{H_{a \rightarrow gg(\gamma\gamma)}}{H_{\text{MD}}} \right)^{\frac{2}{3}} \left(\frac{a(T_{a \rightarrow gg(\gamma\gamma)})}{a(\text{today})} \right), \quad (\text{B11})$$

where we have used that $a \sim H^{-2/3}$ during matter domination. The Hubble rates at the beginning and end of the matter dominated phase can be determined by matching with the radiation dominated expression, i.e. $H \sim T^2/M_p$. One then gets:

$$\omega_{\text{peak, MD}} \simeq \omega_{\text{peak}} \left(\frac{T_{a \rightarrow gg(\gamma\gamma)}}{T_{\text{MD}}} \right)^{\frac{1}{3}}, \quad (\text{B12})$$

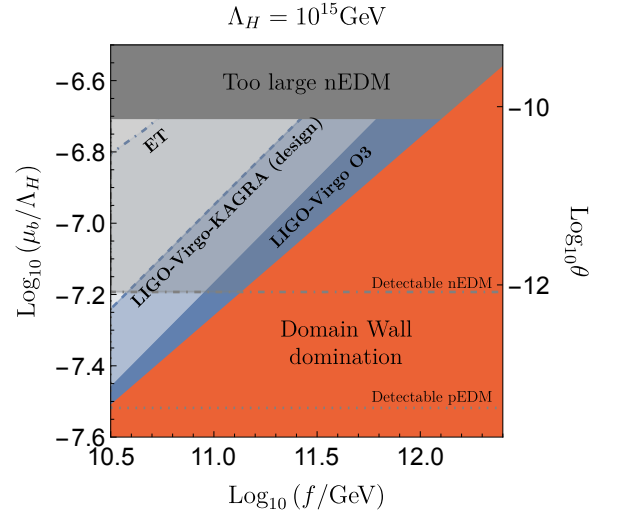


Figure 5. Same as Fig. 1 of the main text, but with $\Lambda_{\text{H}} = 10^{15} \text{ GeV}$ and $\kappa_{\text{H}} = 10^{-9}$.

which shows that the frequency can be much smaller than in the RD case, when $T_{\text{MD}} \gg T_{a \rightarrow gg(\gamma\gamma)}$. The amplitude of the signal is also suppressed by the duration of the MD epoch, i.e.

$$\Omega_{\text{gw,MD}} h^2 \simeq \Omega_{\text{gw}} h^2 \left(\frac{g_*(T_{a \rightarrow gg(\gamma\gamma)})}{g_*(T_{\text{MD}})} \right)^{\frac{1}{3}} \left(\frac{T_{a \rightarrow gg(\gamma\gamma)}}{T_{\text{MD}}} \right)^{\frac{4}{3}}.$$

When the suppression of the amplitude due to MD is not too strong, the gravitational signal can be probed by interferometers which are sensitive at low frequencies, such as DECIGO, LISA and possibly PTAs.

The spectrum of GW waves is characterized by a peak at a frequency ω_{peak} roughly corresponding to the

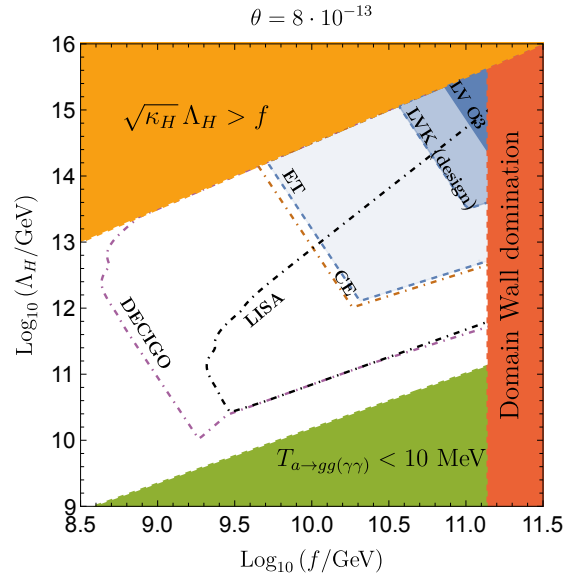


Figure 6. Same as Fig. 2 of the main text, but with $\kappa_{\text{H}} = 10^{-9}$.

horizon at the time of the annihilation of the network, as explained in the main text. For smaller frequencies the spectrum decay as ω^3 , as dictated by causality, whereas for larger frequencies numerical simulations have shown a $1/\omega$ dependence which is cut off at a frequency corresponding to the axion mass [37]. The details of the spectrum near the peak are subject to more uncertainties and motivate further numerical studies. In this work we consider the peak to have a $O(1)\omega_{\text{peak}}$ width, as suggested by numerical simulations, and use the following simple formula for the spectrum to produce Fig. 3 of the main text:

$$\Omega_{\text{gw}}(\omega) = \Omega_{\text{gw}}(\omega_{\text{peak}}) \frac{4}{\left(\frac{\omega}{\omega_{\text{peak}}}\right)^{-3} + 3\left(\frac{\omega}{\omega_{\text{peak}}}\right)} \quad (\text{B13})$$

Smaller widths would not significantly change the predictions. If the peak width is much larger than $O(1)\omega_{\text{peak}}$ the detectability of the signal would significantly improve.

Additionally, we present results for a representative example with $\kappa_{\text{H}} \ll 1$ in Figures 5 and 6. In this case, we take $\sqrt{\kappa_{\text{H}}}f \leq f$ as cutoff of the axion effective theory. Correspondingly, LIGO-Virgo-KAGRA can now probe much larger scales $\Lambda_{\text{H}} \lesssim 10^{15}$ GeV than in the case $\kappa_{\text{H}} = 1$.

Appendix C: Temperature dependent V_b

In the main text we focused on the case where the misaligned contribution to the axion potential is temperature independent. This is typically the case when the source of PQ breaking comes from energy scales above f . Instead, if there are infrared contributions, e.g. coming from sectors which confine at scales $\mu_b \ll f$, the axion potential will be temperature dependent and saturate at temperatures $T_b \lesssim \mu_b$. In this Section we present the results for the latter case and consider a bias potential given by

$$V_b(T) \simeq \mu_b^4(T) \cos\left(\frac{N_b}{N_{\text{DW}}} \frac{a}{f} + \delta\right), \quad (\text{C1})$$

where $\mu_b^4(T) = \mu_b^4 \min\left[\left(\frac{T_b}{T}\right)^n, 1\right]$. When $n = 0$ we recover the case described in the main text. On the other hand, for large n the potential is strongly temperature dependent, the potential approaches a step function and the predictions become almost independent of n . For simplicity, we consider the case of a temperature dependence similar to QCD, i.e. $T_b \lesssim \mu_b$ and $n = 4$. The results are shown in figures 7 and 8 for the same values used in the temperature independent case (see Figures 1 and 2 of the main text).

The main consequence of a temperature dependent bias is that the annihilation of the network will happen at a later temperature $T \lesssim T_b$ thus causing an enhancement

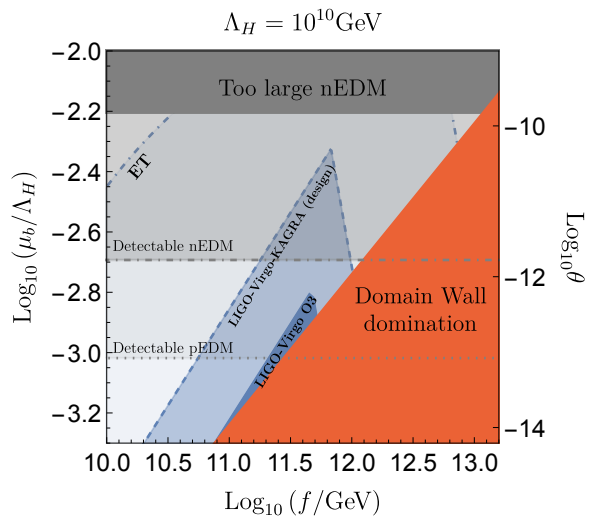


Figure 7. Same as Fig. 1 of the main text, but with a temperature dependent bias.

of the relative energy in the network, $\rho_{\text{dw}}/\rho_{\text{tot}}$, and so on the GW signals. This allows to probe a larger region of parameter space, in particular smaller values of f , simultaneously with nEDM and GW experiments.

Appendix D: Friction

Particles in the primordial plasma that interact with the domain wall can exert thermal friction [56, 63, 94]. This is usually negligible for the QCD axion, since the axion mass is very small compared to the temperature of the plasma, but it can be relevant in the heavy axion scenario. Quantifying these effects is a model-dependent task, since axion interactions are not fixed by the requirement that the axion solves the strong CP problem. Here, we consider a conservative case, where we assume one particle in the plasma to have a probability of order one to be reflected by the axion wall, and show that even in this case friction is only important in a region of parameter space relevant for future interferometers. Even so, we find only a minor impact on the GW signal in this case.

The thermal pressure exerted on the wall by relativistic particle in thermal equilibrium is given by [70]

$$F = P_r n \Delta p \quad (\text{D1})$$

where $n = g_{\text{fr}} \zeta(3) T^3 / \pi^2$ is the density of relativistic particles that are reflected by the wall with a probability P_r , g_{fr} is the number of degrees of freedom and $\Delta p = vT$ the momentum transfer (for non-relativistic walls and after averaging over the two sides of the wall [70]). If the friction caused by the thermal pressure, F/σ , overcomes the Hubble friction, H , the wall will reach an attractor regime where the self-acceleration due to its own tension

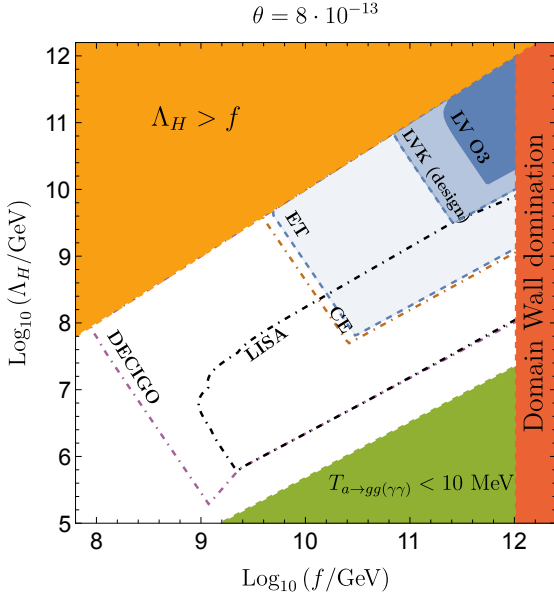


Figure 8. Same as Fig. 2 of the main text, but with temperature dependent bias.

balances the friction force [70]

$$\sigma/R \simeq F. \quad (\text{D2})$$

where R is the typical curvature of the network. In this attractor, the velocity of the wall increases with time as

$$v(t) \simeq 8.7 \left(\frac{1}{g_{\text{fr}} P_r} \right)^{1/2} \left(\frac{\sigma}{M_p T^2} \right)^{1/2} \quad (\text{D3})$$

where we used eq. D1 and $R = vt$. The friction domination regime ends when $F/\sigma \lesssim H$ or, equivalently, when the wall reaches the relativistic limit. Interestingly, when the background is radiation dominated, this always happens at a temperature T_{fr} close to the time of domain wall domination $T_{\text{fr}} \simeq 0.43 \sqrt{g_{\text{fr}} P_r} T_{\text{dw-dom}}$.

Another consequence of thermal friction is the delay of the network annihilation. In the absence of friction, the wall annihilates when the bias pressure overcomes the domain wall tension, $V_b \gtrsim \rho_{\text{dw}}$. However, because R is now smaller due to friction, ρ_{dw} is enhanced and so it will take more time for the bias pressure to dominate and cause the collapse of the network. For a temperature independent bias in a radiation dominated era, that happens when

$$H_{\text{ann}}^{\text{fr}} = 1.2 \left(\frac{g_{*,\text{ann}}}{g_{\text{fr}} P_r} \right)^{1/3} H_{\text{ann}}^{2/3} H_{\text{dom}}^{1/3} < H_{\text{ann}} \quad (\text{D4})$$

where H_{ann} , $H_{\text{dw-dom}}$ are the Hubble rates at the time of domain wall annihilation and domination, respectively, in the absence of friction.

The small velocity of the domain walls also affects the spectrum of gravitational waves. Using the expression for the quadrupole formula one can estimate the power

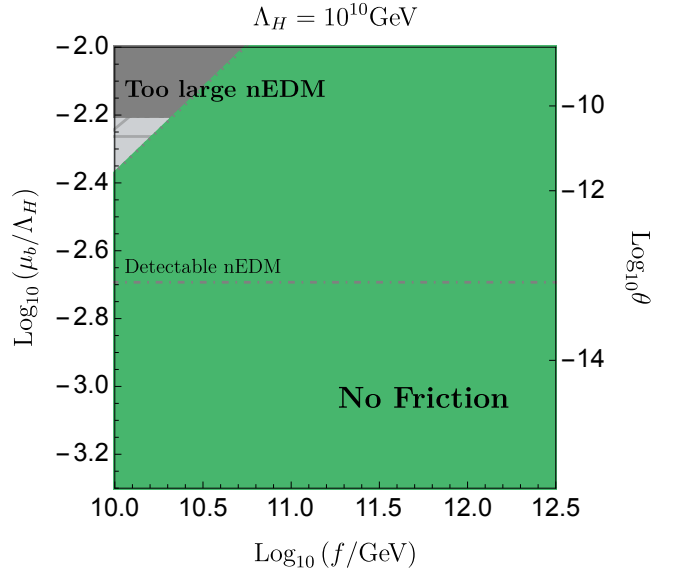


Figure 9. Regions of parameter space where thermal friction on the domain walls from gluons can be neglected, for $\Lambda = 10^{10}$ GeV, using the same choices as for Fig. 1 of the main text.

in gravitational waves at the time of annihilation as [95]

$$P_{\text{GW}}^{\text{fr}} = G \left(\frac{d^3 I}{dt^3} \right)^2 \sim G (v^3 \sigma R)^2_{\text{ann}} \quad (\text{D5})$$

where we used $I \sim \sigma R^4$ for the quadrupole moment of the wall. There are three main changes compared to the frictionless case: i) the amount of gravitational waves is suppressed by $(v^3 R H)^2$, ii) the network annihilates later thus increasing the relative energy in the GWs (when compared to the background), iii) the peak frequency of the spectrum at the time of annihilation is expected to move from $H_{\text{ann}}^{\text{fr}}$ to $1/R_{\text{ann}}^{\text{fr}}$.

What remains to assess is the value of the reflection probability P_r . To do that we need to specify the interactions of the axion with the plasma. At temperatures above 1 GeV, the focus of this work, there is one unavoidable interaction due to the axion coupling to gluons. Other interactions are also possible, for example with SM fermions, which can be sizeable in DFSZ-like constructions, or with particles in the dark sector (both in the bias or in Λ_H), but those are model dependent.

Here we will take a conservative approach and assume the reflection probability to be maximal, $P_r = 1$. We will present a more detailed analysis of friction due to gluons in [89]. In Figs. 9 and 10 we show the region of parameter space where friction is important, assuming $g_{\text{fr}} = 1$, and the respective prediction for the GW spectrum. In order to perform a fair comparison with the frictionless case, we also included the numerical factors c, d, β in the expressions for friction. The results show that friction is only relevant in a small region of parameter space which is bounded by the condition that the network annihilates

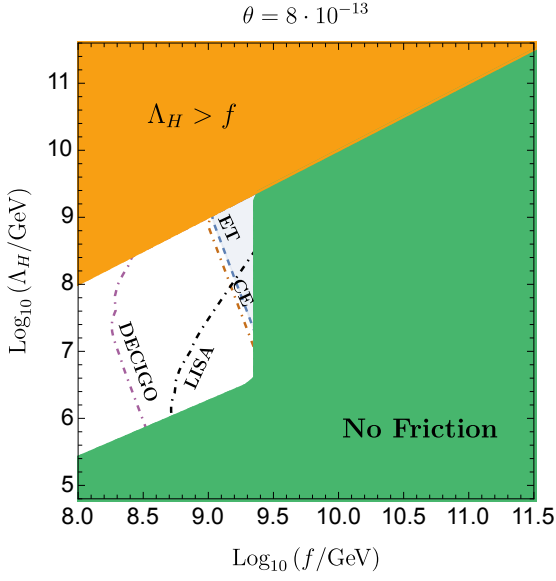


Figure 10. Regions of parameter space where thermal friction on the domain walls from gluons can be neglected, for $\theta = 8 \cdot 10^{-13}$, using the same choices as for Figure 2 of the main text. Regions that can be probed by GW interferometers are also shown in the regions where friction is important and is thus included in the calculation.

during the friction domination regime $T^{\text{fr}} < T_{\text{ann}}^{\text{fr}}$ and by the requirement that $T_{\text{ann}}^{\text{fr}} < m_a$, otherwise the reflection probability will be suppressed. Even in the corner where friction is relevant, the predictions are only mildly different from those without friction (c.f. Figs.1 and 2 of the main text).

Appendix E: $N_{\text{DW}} = 1$

Here we discuss the case $N_{\text{DW}} = 1$ in some more detail. In contrast with the case $N_{\text{DW}} > 1$, the network is unstable even in the absence of extra sources of PQ breaking, see e.g. [58] and [37, 64] for numerical simulations. Annihilation occurs once the energy density in strings is comparable to that in domain walls. The energy density of strings is $\rho_s \simeq \lambda \mu H^2$, where $\mu = \pi f^2 \log(t f / \sqrt{\lambda})$ is the string tension, t is time, and $\lambda \simeq 4$ is a parameter that can be determined via numerical simulations. Deviations from this regime that have been observed in the literature [59, 61] are not

particularly relevant to us, since in the heavy axion scenario strings only evolve until $\Lambda_H \gg \Lambda_{\text{QCD}}$. By equating to $\rho_{\text{dw}} = c\sigma(T)H$ (for $N_{\text{DW}} = 1$, $c \approx 1$ [64]), one finds the annihilation temperature, which also depends on the temperature dependence of the heavy axion potential. We follow here the same example choice as in Appendix B, although this does not affect our conclusions.

$$T_{\text{ann}} \simeq 10^{10} \text{ GeV} \left(\frac{2\kappa_H c}{\lambda} \right)^{\frac{1}{6}} \left(\frac{106.75}{g_*} \right)^{\frac{1}{12}} \times \left(\frac{10^{15} \text{ GeV}}{f} \right)^{\frac{1}{6}} \left(\frac{\Lambda_H}{10^{10} \text{ GeV}} \right). \quad (\text{E1})$$

Following the same steps as in Appendix B, and assuming radiation domination below T_{ann} , the gravitational wave peak frequency is found to be

$$\omega_{\text{peak}} \simeq 10^3 \text{ Hz} \left(\frac{\lambda \kappa_H}{4} \right)^{\frac{1}{6}} \left(\frac{T_0/\Lambda_H}{0.4} \right)^{\frac{2}{3}} \left(\frac{106.75}{g_{*,\text{ann}}} \right)^{\frac{1}{12}} \times \left(\frac{10^{15} \text{ GeV}}{f} \right)^{\frac{1}{6}} \left(\frac{\Lambda_H}{10^{10} \text{ GeV}} \right), \quad (\text{E2})$$

while the peak amplitude of the gravitational wave signal is given by

$$\Omega_{\text{gw}} h^2 \simeq 10^{-17} \tilde{c} \left(\frac{\lambda}{4} \right)^2 \left(\frac{106.75}{g_{*,\text{ann}}} \right)^{\frac{1}{3}} \left(\frac{f}{10^{15} \text{ GeV}} \right)^4. \quad (\text{E3})$$

From the formulae above, it appears to be possible to obtain a visible signal (at future interferometers) only when $f \lesssim 10^{16} \text{ GeV}$ and $\Lambda_H < 10^{10} \text{ GeV}$. In fact, there are two problems with these choices: First, such large values of f may generally lead to PQ symmetry being never restored after inflation, since the current upper bound on the reheating temperature after inflation is $T \lesssim 10^{16} \text{ GeV}$. Secondly, reducing Λ_H reduces the axion mass, which can then lead to a slower decay rate to SM states and an intermediate phase of MD, which has not been taken into account in deriving the equations above. When relevant, this suppresses the gravitational wave signal further. Overall, when including these effects, we find no observable region of parameter space for $N_{\text{DW}} = 1$.